Capillary levelling of free-standing liquid nanofilms

Mark Ilton,[1] Miles M. P. Couchman,[1] Thomas Salez,[2] Michael Benzaquen,[2] Paul D. Fowler,[1] Elie Raphaël,[2] and Kari Dalnoki-Veress[1, 2, *]

[1] *Department of Physics & Astronomy, McMaster University, Hamilton, Ontario, Canada, L8S 4M1*
[2] *Laboratoire de Physico-Chimie Théorique, UMR CNRS Gulliver 7083, ESPCI ParisTech, PSL Research University, 75005 Paris, France*

(Dated: February 18, 2016)

We report on the capillary-driven levelling of a topographical perturbation at the surface of a free-standing liquid nanofilm. The width of a stepped surface profile is found to evolve as the square root of time. A hydrodynamic model which assumes plug flow is in excellent agreement with the experimental data. In addition to exhibiting a striking analogy with diffusive processes, this novel system serves as a precise nanoprobe for the rheology of liquids at interfaces in a configuration that avoids substrate effects, and allows for a first test of the theoretical descriptions of strong-slip flows.

Continuum fluid dynamics provides a remarkably accurate description of flows from nanometric to astronomical length scales, and can accommodate a variety of effects and forces such as inertia, gravity, surface tension, viscosity, etc. Capillary-driven flows mediated by viscosity represent a particularly interesting situation as these two mechanisms dominate at small length scales and thus in several technologically-relevant applications [1, 2]. They also underlie conceptually simple experiments that probe physics at interfaces and in confinement, such as the molecular motion of fluid particles at a solid boundary [3], or the universal coalescence of droplets [4]. Moreover, the thin-film geometry allows for an important simplification since the in-plane flow dominates [5]. In this so-called lubrication approximation, dynamics are solely controlled by the ratio of the film-air surface tension to viscosity, known as the capillary velocity $v_c = \gamma/\eta$, and the film thickness which sets the characteristic length scale.

Until now, research has been largely focused on thin films *supported* on solid substrates [6–9]. One way to probe the dynamics of such a film is to apply an external stress and to measure the departure from the initial state. Measurements can be achieved through a variety of experimental techniques, such as the dynamic surface forces apparatus [10] including substrate elasticity [11], nanoparticle embedding [12–14], electrohydrodynamic instability [15–18], unfavorable wetting conditions [3, 19–25], and Marangoni flow [26–29]. Alternatively, the dynamics of a thin coating of liquid can be probed by starting with an out-of equilibrium surface topography and observing the film as it relaxes towards equilibrium [30–44]. All the above approaches can be used to study physical properties such as the glass transition [12–14, 32, 34, 43], viscoelasticity [39, 42], and interfacial molecular friction [3, 24, 25].

In contrast to these studies, one could examine capillary-driven flows mediated by viscosity in a configuration with no substrate effect: a *free-standing* film. Flow in such a geometry has been previously studied for liquids with some internal structure that stabilizes the film against rupture, such as soap films [45–50], or liquid-crystal films [51–53], but this structure has necessarily a significant impact on the dynamics. Designing homogeneous isotropic free-standing liquid nanofilms presents experimental challenges in their creation, stability, and observation, as the techniques used for supported films typically do not work. Nevertheless, this geometry remains highly compelling as a way to study fundamental phenomena without any substrate-induced artifact. For instance, the glass-transition temperature reductions observed for supported films [54] are more pronounced for free-standing films [55, 56]. Also, due to the absence of any liquid-substrate interaction, confinement effects of polymeric liquids [57–60] may be addressed in an ideal way using free-standing films [61, 62]. Finally, the boundaries of a free-standing film are the perfect realization of strong-slip interfaces, and can serve as first experimental tests of the associated theoretical predictions [63, 64].

In this Letter, we report on a novel capillary-levelling experiment involving free-standing stepped nanofilms. First, using atomic force microscopy (AFM), we empirically determine the scaling law for the width evolution of the prepared samples. Then, invoking hydrodynamics, we derive a free-standing thin-film equation showing excellent agreement with experimental data. The only adjustable parameter is the capillary velocity, which allows the system to be used as a rheological nanoprobe. Finally, by performing simultaneous experiments on both supported and free-standing films, we self-consistently confirm the robustness of the technique.

Free-standing stepped films are prepared using a similar protocol as developed for supported films [65]. Here, thin polystyrene (PS) films, with thickness in the $100 - 500\,\mathrm{nm}$ range, are spincoated from dilute PS (Polymer Source, Canada, with weight-averaged molecular weight 55 kg/mol) solution in toluene onto freshly cleaved mica (Ted Pella, USA), and pre-annealed for at least ten minutes on a hot stage (Linkham, UK) at $140\,^{\circ}\mathrm{C}$, well above the glass-transition temperature $T_g \approx 100\,^{\circ}\mathrm{C}$ of the ma-

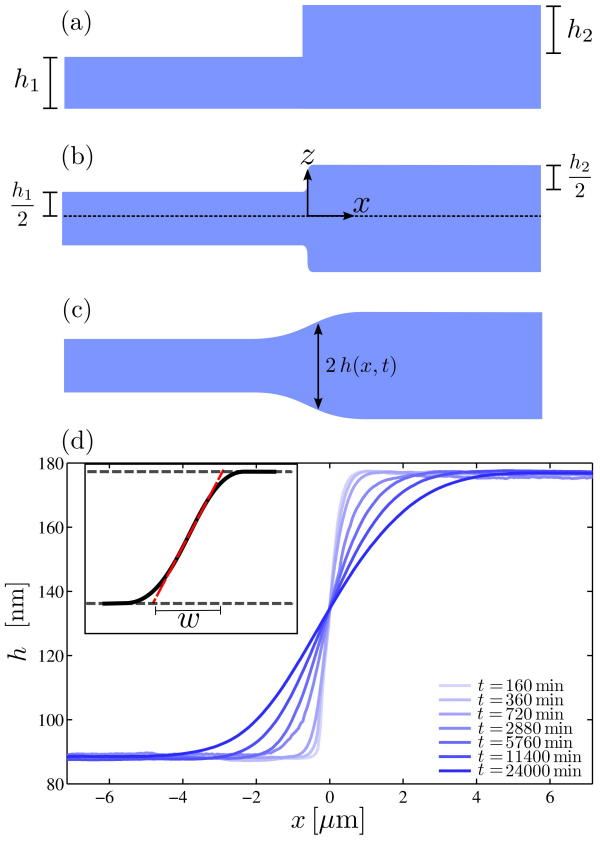

FIG. 1. (a) Schematic of a free-standing stepped film. (b) In the melt state, the profile quickly symmetrizes with respect to the central plane (dotted line) at $z = 0$. (c) The two mirrored steps broaden horizontally over time. The half-height profile $h(x, t)$ is recorded with AFM. (d) AFM profiles of a free-standing stepped film with $h_1 = h_2 = 176\,\text{nm}$, for different times t spent above T_g. As sketched in the inset (arbitrary units), the profile width w is defined from the tangent (tilted dashed) line in the middle of the step and the film thickness.

terial. After annealing, the films are floated onto a deionized water bath (18.2 MΩ cm, Pall, USA) and picked up onto custom-machined stainless steel grids. Each grid has 85 hexagonal holes ($\sim 1\,\text{mm}$ across) which allows the simultaneous preparation of ~ 85 isolated free-standing samples. All results described here are obtained from the few films that remain stable against spontaneous rupture over the course of the entire experiment. After floating a film with thickness h_1 onto the grid, it is heated above T_g to remove wrinkles. A second film with thickness h_2 and a sharp edge [66] is then floated atop the first film, as schematically shown in Fig. 1(a). The free-standing stepped film is then annealed at 110 °C on the hot stage for a time t. To vertically equilibrate the pressure, the film rapidly symmetrizes into two mirrored steps as depicted in Fig. 1(b). Because the vertical length scale is orders of magnitude smaller than the typical horizontal one, the vertical symmetrization occurs rapidly on experimental time scales and is not resolved.

The presence of an excess interfacial area with respect to the flat equilibrium state drives flow, thus causing the profile to broaden laterally over time, as shown schematically in Fig. 1(c). The speed of this relaxation is given by the capillary velocity. Each film is cooled rapidly ($> 90\,°\text{C/min}$) from 110 °C to room temperature, deep into the glassy state, and then imaged using AFM (Veeco Caliber, USA), with all sources of vibrations minimized. After imaging, the sample is placed back on the hot stage and rapidly heated above T_g to continue its levelling process. Because appreciable flow does not occur at room temperature, the film can be intermittently imaged this way.

Previous experiments on stepped films supported on a substrate [38] have shown that the width w of the profile increases with a 1/4 power law in time:

$$w \propto \left(v_\text{c} h_2^3 t\right)^{1/4} \quad \text{[supported film]}\ , \tag{1}$$

where h_2 is the thickness of the top film as in Fig 1(a), and where the missing numerical prefactor depends on the aspect ratio h_2/h_1. Equation (1) is obtained from the capillary-driven thin-film equation [5, 8, 9], which results from the incompressible Stokes equation in the lubrication approximation, together with a no-slip boundary condition at the solid-liquid interface and no shear stress at the liquid-air interface. In that case, there is a Poiseuille flow with a *parabolic velocity profile*.

For the free-standing stepped-film experiments studied here, a typical temporal evolution is shown in Fig. 1(d). To characterize the broadening, the width w of the profile [65] is defined (Fig. 1(d), inset) and recorded as a function of time. As seen in Fig. 2, the evolution is consistent with a $t^{1/2}$ power law. Also shown are the results for two other thicknesses (keeping $h_1 = h_2$). Each dataset is then fit to $w = (Mt)^{1/2}$, where the mobility M is a free parameter that is found to scale linearly with h_2 (Fig. 2, inset). Using dimensional analysis, this empirically gives:

$$w \propto \left(v_\text{c} h_2 t\right)^{1/2} \quad \text{[free-standing film]}\ , \tag{2}$$

where the missing prefactor is expected to depend on h_2/h_1. This scaling is similar to Eq. (1), but with a different power-law exponent. There is a stronger dependence on time in free-standing films compared to supported films, which is consistent with the former flowing more easily due to the unconstrained boundaries.

Motivated by the empirical scaling of Eq. (2), we now turn to a theoretical description. Let us consider a symmetric free-standing stepped film of total thickness $2\,h(x, t)$ (Fig. 1(c)), that viscously flows under the action of liquid-air surface tension. We denote $u(x, z, t)$ the fluid velocity along x, and we assume the problem to be invariant along the other horizontal direction. By symmetry, we limit ourselves to $z > 0$, and in the central plane ($z = 0$) we have:

$$\partial_z u|_{z=0} = 0\ . \tag{3}$$

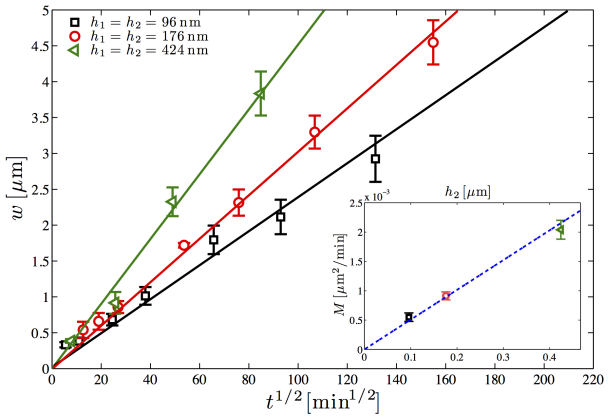

FIG. 2. Profile width w (Fig. 1(d), inset) as a function of the square root of time $t^{1/2}$, for free-standing stepped films with $h_1 = h_2$. The open symbols are the measured widths for three different film thicknesses, as indicated. The solid lines are fits to $w = (Mt)^{1/2}$, where the mobility M is the fitting parameter. (inset) Mobility as a function of thickness h_2, when $h_1 = h_2$. The dashed line is a linear fit.

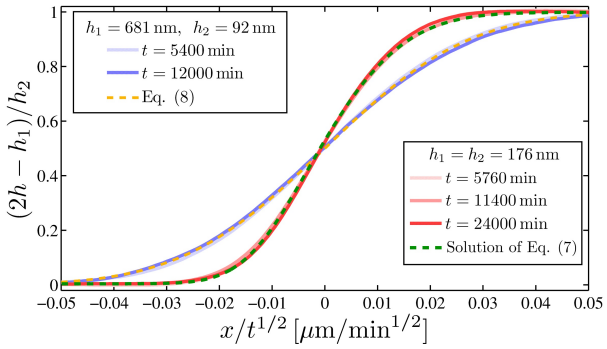

FIG. 3. Normalized long-term experimental height profiles as a function of the self-similar variable, at several times and for two different geometries as indicated. The dark dashed line indicates a fit using the numerical solution of Eq. (7) for the $h_1 = h_2$ case. The light dashed line represents a fit using Eq. (8).

Since the air viscosity is negligibly small compared to the film viscosity, there is no shear stress at the liquid-air interface ($z = h$). There, the continuity of tangential and normal stresses reads:

$$\partial_z u|_{z=h} = 0 \tag{4}$$

$$p|_{z=h} = -\gamma \partial_x^2 h - 2\eta \partial_x u|_{z=h} \ , \tag{5}$$

where $p(x, z, t)$ is the pressure difference in the film with respect to the atmospheric value, and where we invoked incompressibility, the Young-Laplace equation and the small-slope approximation ($\partial_x h \ll 1$). As a consequence, and in contrast to supported films, the flow cannot be of Poiseuille type. In view of Eqs. (3) and (4), and given the thin-film geometry ($h \ll w$ at all studied times), we assume a *plug flow* – *i.e.* a purely horizontal flow with $u = u(x, t)$ – to be rapidly reached. With this simplification, the Stokes equation reads:

$$\eta \partial_x^2 u = \partial_x p \ . \tag{6}$$

Integrating Eq. (6) twice with respect to x, while evaluating $p = p(x, t)$ through Eq. (5), leads to $u = -\frac{v_c}{3}\partial_x h$. The two constants of integration are set to zero, since far away from the step there is no flow and the film is flat. Invoking volume conservation, $\partial_t h = -\partial_x(hu)$, leads to the free-standing thin-film equation:

$$\partial_t h = \frac{v_c}{3}\partial_x(h\,\partial_x h) \ . \tag{7}$$

Interestingly, this equation describes the 1D diffusion of the profile h, with a non-constant diffusion coefficient $v_c h/3$ that is proportional to h. As such, Eq. (7) admits self-similar solutions in the variable $x/t^{1/2}$ [67, 68]. Assuming that the initial profile of Fig. 1(b) leads to such a self-similar solution, one gets by dimensional analysis that $h(x, t) = h_1 f[x/(h_2 v_c t)^{1/2}, h_2/h_1]$, where f is an unknown dimensionless function of two variables. This corroborates the empirical horizontal scaling of Eq. (2).

By employing a finite-difference scheme [69], numerical solutions of Eq. (7) for stepped initial profiles are computed and fit to the experimental data. Figure 3 shows the rescaled long-term experimental profiles of the $h_1 = h_2 = 176$ nm geometry of Fig. 1(d). The normalized height is plotted against the self-similar variable $x/t^{1/2}$, for three different annealing times. The profiles collapse onto a single master curve – thus confirming self-similarity – and are in full agreement with the numerical solution. The vertical discrepancy is less than 1 nm, and there is a similar level of agreement for the two other geometries of Fig. 2. The single fit parameter v_c will be studied in detail below.

Furthermore, when the initial stepped profile of Fig. 1(b) is such that $h_2 \ll 2h_1$, Eq. (7) can be linearized into a standard diffusion equation and its analytical solution thus reads:

$$h(x, t) = \frac{h_1}{2} + \frac{h_2}{4}\left[1 + \mathrm{erf}\left(\sqrt{\frac{3x^2}{(2h_1 + h_2)v_c t}}\right)\right] \ . \tag{8}$$

As seen in Fig. 3, Eq. (8) fits the experimental data remarkably well for a sample with $h_1 = 681$ nm and $h_2 = 92$ nm.

A final self-consistency check is performed in order to ensure the accuracy on the single fit parameter v_c extracted from the comparison with theory. As a material property of the film in contact with air, it should not depend on the presence of an additional substrate-film interface. Stepped PS films (55 kg/mol, $h_1 = h_2 = 390$ nm) are thus prepared in free-standing and substrate-supported (Silicon wafers or $\sim 4\mu$m-thick polysulfone films) configurations. Both are annealed side-by-side, at

the same time, in a home-built vacuum oven at 120 °C. The profiles are measured after 735 and 1485 minutes to confirm self-similarity. Figure 4(a) shows the results for the supported case. The normalized height profile is plotted as a function of the self-similar variable $x/t^{1/4}$ of Eq. (1). The numerical profile [69] is fit to the experimental data with one single free parameter: $v_c = 0.068 \pm 0.008\,\mu$m/min. Figure 4(b) shows the results for the free-standing case. The normalized height profile is plotted as a function of the self-similar variable $x/t^{1/2}$ of Eq. (2). The numerical solution of Eq. (7) is fit to the experimental data with one single free parameter: $v_c = 0.065 \pm 0.005\,\mu$m/min. Together with the excellent fit qualities, the fact that both cases give accurately the same capillary velocity proves: i) the robustness of the free-standing stepped-film technique as a precise rheological nanoprobe, and ii) the validity of the free-standing thin-film equation (Eq. (7)) and its simple underlying plug-flow assumption. Interestingly, Eq. (7) appears to be different from the infinite-slip limit of previous predictions [63, 64], which could be attributed to either the specific initial condition used here, or the unresolved difference between the two descriptions with our current precision.

In conclusion, we report on flow in free-standing stepped nanofilms. Above the glass-transition temperature, the surface profiles broaden with a characteristic $t^{1/2}$ power law, as measured by AFM. Unlike substrate-supported films with a no-slip liquid-solid boundary condition, the levelling is consistent with a plug-flow assumption. A free-standing thin-film equation, different from previous infinite-slip predictions, is found to be in excellent agreement with experimental data. Finally, the capillary velocity γ/η is robustly and accurately extracted from the comparison with theory. We expect this novel system to be of fundamental interest for three reasons: first, it presents a striking analogy with nonlinear diffusive processes; secondly, it embodies a perfect realization of strong-slip interfaces and, as such, is the first test of the associated theoretical predictions; thirdly, by avoiding any substrate-induced artifact, it serves as a precise nanoprobe for addressing fundamental questions about complex fluids and glass formers in confinement and at interfaces.

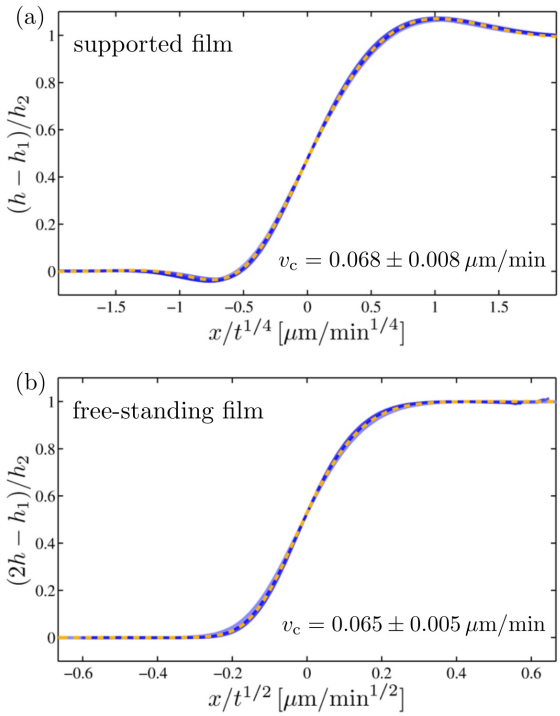

FIG. 4. (a) Normalized long-term experimental height profiles (solid lines) of supported stepped films as a function of the self-similar variable $x/t^{1/4}$ of Eq. (1), for ten samples and two different times. The numerical solution [69] is fit (dashed line) to the experimental profiles, with v_c as the free parameter. (b) Normalized long-term experimental height profiles (solid lines) of free-standing stepped films as a function of the self-similar variable $x/t^{1/2}$ of Eq. (2), for twelve samples and two different times. The numerical solution of Eq. (7) is fit (dashed line) to the experimental profiles, with v_c as the free parameter.

* dalnoki@mcmaster.ca

[1] P. Tabeling, *Introduction to Microfluidics* (Oxford University Press, 2005).

[2] K. Jacobs, R. Seemann, and S. Herminghaus, in *Polym. Thin Film.*, edited by O. K. C. Tsui and T. P. Russell (World Scientific, 2008) Chap. 10, pp. 243–265.

[3] O. Bäumchen and K. Jacobs, J. Phys. Condens. Matter **22**, 033102 (2010).

[4] J. F. Hernández-Sánchez, L. A. Lubbers, A. Eddi, and J. H. Snoeijer, Phys. Rev. Lett. **109**, 184502 (2012).

[5] R. Blossey, *Thin Liquid Films: Dewetting and Polymer Flow* (Springer, 2012).

[6] L. E. Stillwagon and R. G. Larson, Journal of Applied Physics **63?5251** (1988).

[7] L. E. Stillwagon and R. G. Larson, Physics of Fluids A: Fluid Dynamics **2?1937** (1990).

[8] A. Oron, S. Davis, and S. Bankoff, Rev. Mod. Phys. **69**, 931 (1997).

[9] R. Craster and O. Matar, Rev. Mod. Phys. **81**, 1131 (2009).

[10] J. N. Israelachvili, P. M. McGuiggan, and A. M. Homola, Science **240**, 189 (1988).

[11] R. Villey, E. Martinot, C. Cottin-Bizonne, M. Phaner-Goutorbe, L. Léger, F. Restagno, and E. Charlaix, Phys. Rev. Lett. **111**, 215701 (2013).

[12] J. H. Teichroeb and J. A. Forrest, Phys. Rev. Lett. **91**, 016104 (2003).

[13] M. Ilton, D. Qi, and J. A. Forrest, Macromolecules **42**, 6851 (2009).

[14] D. Qi, M. Ilton, and J. A. Forrest, Eur. Phys. J. E. Soft Matter **34**, 1 (2011).

[15] E. Schaffer, T. Thurn-Albrecht, T. Russell, and

U. Steiner, Nature **403**, 874 (2000).
[16] M. D. Morariu, N. E. Voicu, E. Schäffer, Z. Lin, T. P. Russell, and U. Steiner, Nat. Mater. **2**, 48 (2003).
[17] N. Voicu, S. Harkema, and U. Steiner, Adv. Funct. Mater. **16**, 926 (2006).
[18] D. R. Barbero and U. Steiner, Phys. Rev. Lett. **102? 248303** (2009).
[19] D. J. Srolovitz and S. A. Safran, J. Appl. Phys. **60**, 255 (1986).
[20] F. Wyart and J. Daillant, Can. J. Phys. **68**, 1084 (1990).
[21] R. Seemann, S. Herminghaus, and K. Jacobs, Phys. Rev. Lett. **87**, 196101 (2001).
[22] G. Reiter, M. Hamieh, P. Damman, S. Sclavons, S. Gabriele, T. Vilmin, and E. Raphaël, Nat. Mater. **4**, 754 (2005).
[23] X.-C. Chen, H.-M. Li, F. Fang, Y.-W. Wu, M. Wang, G.-B. Ma, Y.-Q. Ma, D.-J. Shu, and R.-W. Peng, Adv. Mater. **24**, 2637 (2012).
[24] O. Bäumchen, R. Fetzer, and K. Jacobs, Phys. Rev. Lett. **103**, 1 (2009).
[25] O. Bäumchen and K. Jacobs, Soft Matter **6**, 6028 (2010).
[26] C. B. Kim, D. W. Janes, D. L. McGuffin, and C. J. Ellison, J. Polym. Sci. Part B Polym. Phys. **52**, 1195 (2014).
[27] J. M. Katzenstein, C. B. Kim, N. A. Prisco, R. Katsumata, Z. Li, D. W. Janes, G. Blachut, and C. J. Ellison, Macromolecules **47**, 6804 (2014).
[28] T. A. Arshad, C. B. Kim, N. A. Prisco, J. M. Katzenstein, D. W. Janes, R. T. Bonnecaze, and C. J. Ellison, Soft Matter **10**, 8043 (2014).
[29] J. M. Katzenstein, D. W. Janes, J. D. Cushen, N. B. Hira, D. L. McGuffin, N. A. Prisco, and C. J. Ellison, ACS Macro Lett. , 1150 (2012).
[30] O. K. C. Tsui, Y. J. Wang, F. K. Lee, C.-H. Lam, and Z. Yang, Macromolecules **41**, 1465 (2008).
[31] Z. Yang, C. H. Lam, E. Dimasi, N. Bouet, J. Jordan-Sweet, and O. K. C. Tsui, Appl. Phys. Lett. **94**, 3 (2009).
[32] Z. Yang, Y. Fujii, F. K. Lee, C.-H. Lam, and O. K. C. Tsui, Science **328**, 1676 (2010).
[33] F. Chen, D. Peng, C.-H. Lam, and O. K. C. Tsui, Macromolecules , 150709130643005 (2015).
[34] Z. Fakhraai and J. A. Forrest, Science **319**, 600 (2008).
[35] T. Leveder, S. Landis, and L. Davoust, Appl. Phys. Lett. **92**, 013107 (2008).
[36] T. Leveder, E. Rognin, S. Landis, and L. Davoust, Microelectron. Eng. **88**, 1867 (2011).
[37] E. Rognin, S. Landis, and L. Davoust, Phys. Rev. E **84**, 041805 (2011).
[38] J. D. McGraw, T. Salez, O. Bäumchen, E. Raphaël, and K. Dalnoki-Veress, Phys. Rev. Lett. **109**, 128303 (2012).
[39] E. Rognin, S. Landis, and L. Davoust, J. Vac. Sci. Technol. B Microelectron. Nanom. Struct. **30**, 011602 (2012).
[40] M. Backholm, M. Benzaquen, T. Salez, E. Raphaël, and K. Dalnoki-Veress, Soft Matter **10**, 2550 (2014).
[41] M. Benzaquen, P. Fowler, L. Jubin, T. Salez, K. Dalnoki-Veress, and E. Raphaël, Soft Matter **10**, 8608 (2014).
[42] E. Rognin, S. Landis, and L. Davoust, Langmuir **30**, 6963 (2014).
[43] Y. Chai, T. Salez, J. D. McGraw, M. Benzaquen, K. Dalnoki-Veress, E. Raphaël, and J. A. Forrest, Science **343**, 994 (2014).
[44] M. Benzaquen, M. Ilton, M. V. Massa, T. Salez, P. Fowler, E. Raphaël, and K. Dalnoki-Veress, Appl. Phys. Lett. **107**, 053103 (2015).
[45] M. A. Rutgers, X.-l. Wu, R. Bhagavatula, A. A. Petersen, and W. I. Goldburg, Phys. Fluids **8**, 2847 (1996).
[46] V. Horváth, J. Cressman, W. Goldburg, and X. Wu, Phys. Rev. E **61**, R4702 (2000).
[47] D. Georgiev and P. Vorobieff, Rev. Sci. Instrum. **73**, 1177 (2002).
[48] H. Diamant, J. Phys. Soc. Japan **78**, 041002 (2009).
[49] J. Seiwert, M. Monloubou, B. Dollet, and I. Cantat, Phys. Rev. Lett. **111**, 094501 (2013).
[50] M. J. Huang, C. Y. Wen, I. C. Lee, and C. H. Tsai, Phys. Fluids **16**, 3975 (2004).
[51] K. Harth, A. Eremin, and R. Stannarius, Soft Matter **7**, 2858 (2011).
[52] A. Eremin, C. Bohley, and R. Stannarius, Phys. Rev. E - Stat. Nonlinear, Soft Matter Phys. **74**, 1 (2006).
[53] R. Stannarius, C. Bohley, and A. Eremin, Phys. Rev. Lett. **97**, 1 (2006).
[54] J. L. Keddie, R. A. L. Jones, and R. A. Cory, EPL (Europhysics Letters) **27**, 59 (1994).
[55] J. A. Forrest, K. Dalnoki-Veress, J. R. Stevens, and J. R. Dutcher, Physical Review Letters **77**, 2002 (1996).
[56] O. Bäumchen, J. D. McGraw, J. A. Forrest, and K. Dalnoki-Veress, Physical Review Letters **109**, 055701 (2012).
[57] A. Silberberg, J. Colloid Int. Sci. **90?86** (1982).
[58] F. Brochard Wyart and P.-G. de Gennes, Eur. Phys. J. E **1?93** (2000).
[59] H. Bodiguel and C. Fretigny, Phys. Rev. Lett. **97?266105** (2006).
[60] K. Shin, S. Obukhov, J.-T. Chen, J. Huh, Y. Hwang, S. Mok, P. Dobriyal, P. Thiyagarajan, and T. Russell, Nature Materials **6?961** (2007).
[61] Dalnoki-Veress, K., Forrest, J. A., de Gennes, P. G., and Dutcher, J. R., J. Phys. IV France **10**, Pr7 (2000).
[62] L. Si, M. V. Massa, K. Dalnoki-Veress, H. R. Brown, and R. A. L. Jones, Phys. Rev. Lett. **94?127801** (2005).
[63] K. Kargupta, A. Sharma, and R. Khanna, Langmuir **20?244** (2004).
[64] A. Münch, B. Wagner, and T. P. Witelski, Jour. Eng. Math. **53**, 359 (2005).
[65] J. D. McGraw, N. M. Jago, and K. Dalnoki-Veress, Soft Matter **7**, 7832 (2011).
[66] O. Bäumchen, M. Benzaquen, T. Salez, J. D. McGraw, M. Backholm, P. Fowler, E. Raphaël, and K. Dalnoki-Veress, Phys. Rev. E **88**, 035001 (2013).
[67] J. Fourier, *Théorie analytique de la chaleur* (Firmin Didot, père et fils, Paris, 1822).
[68] G. I. Barenblatt, *Scaling, self-similarity, and intermediate asymptotics* (Cambridge University Press, Cambridge, 1996).
[69] T. Salez, J. D. McGraw, S. L. Cormier, O. Bäumchen, K. Dalnoki-Veress, and E. Raphaël, Eur. Phys. J. E **35**, 114 (2012).